CHEMISTRY
A EUROPEAN JOURNAL

DOI: 10.1002/chem.200501463

The Reaction Mechanism of a Complex Intercalation System: In Situ X-ray Diffraction Studies of the Chemical and Electrochemical Lithium Intercalation in Cr_4TiSe_8

Malte Behrens,[a] Ragnar Kiebach,[a] Jannes Ophey,[a] Oliver Riemenschneider,[b] and Wolfgang Bensch*[a]

Abstract: The intercalation reaction between Cr_4TiSe_8 and Li was investigated from a kinetic and an electrochemical perspective. The structural phase transition from monoclinic to trigonal symmetry was probed by in situ energy-dispersive X-ray diffraction (in situ EDXRD) for chemical intercalation with butyllithium (BuLi). A change in the kinetic mechanism was detected for the reaction at room temperature; this was interpreted in terms of a trend from phase boundary control to diffusion control. A single diffusion-controlled mechanism is obeyed at 60 °C. The electrochemical measurements and the corresponding in situ X-ray diffraction (in situ XRD) data revealed that the monoclinic host is intercalated up to the composition $Li_{x\approx0.1}Cr_4TiSe_8$ before the characteristic phase transition starts. The monoclinic phase undergoes complex structural changes in the following two-phase regime. Owing to the co-existence of two phases, the cell potential is constant for $0.1 < x < 0.7$ and $0.9 < x < 3.0$. The subsequent intercalation into the trigonal phase leads to a pronounced increase in the cell volume of the trigonal phase that stops at $x \approx 0.8$. At this point, the complete reduction of Ti^{IV} gives rise to a voltage drop of the cell potential. XANES measurements revealed that the reduction of Ti^{IV} occurs prior to the reduction of Cr^{III}.

Keywords: intercalation · kinetics · solid-state reactions · transition-metal selenides · X-ray scattering

Introduction

Intercalation chemistry requires a reaction temperature that allows the necessary diffusion of the guests into the host matrix. On the other hand, the temperature is limited by the stability of the host with respect to decomposition to keep the reactants in a pseudobinary reaction system of guest and host.[1,2] Typical reaction temperatures for intercalation reactions are at or around room temperature.[3] This makes intercalation chemistry a "soft chemistry" compared to high-temperature solid-state reactions that are governed by thermodynamics.[4] Such low-temperature chemistry allows not only access to metastable products but also provides valuable insights into the reaction mechanisms and its kinetics by applying in situ methods.[5–8]

The complex transition-metal selenide Cr_4TiSe_8 was shown to be a suitable host system for chemical intercalation with butyllithium (BuLi) as the Li source. It accepts up to 2.8 Li atoms per formula unit.[9] One highly interesting feature of this intercalation reaction is the irreversible structural phase transition of the host matrix from monoclinic to trigonal symmetry (Figure 1). The lithiated phase can also be obtained in an electrochemical cell reaction in which the host material is an insertion electrode versus elemental Li. The reaction product of both reaction pathways is trigonal $Li_{x'}CrTi_{0.25}Se_2$ ($x' = x/4$), which has a structure that is closely related to intercalated, layered transition-metal dichalcogenides (TMDCs) and displays an enhancement of this frequently studied class of materials. In $Li_{x'}CrTi_{0.25}Se_2$, the van der Waals gaps between the $Cr_{0.75}Ti_{0.25}Se_2$ slabs are occupied by 0.25 Cr atoms,[10] and the compound may thus be regarded as a partly self-intercalated TMDC. Studies on the reactions of alkali-metal intercalation in TMDCs have notably contributed to the understanding of intercalation chemistry

[a] Dipl.-Chem. M. Behrens, Dr. R. Kiebach, J. Ophey, Prof. Dr. W. Bensch
Institut für Anorganische Chemie, University of Kiel
Olshausenstrasse 40–60, 24098 Kiel (Germany)
Fax: (+49) 341-880-1520
E-mail: wbensch@ac.uni-kiel.de

[b] Dr. O. Riemenschneider
Present address: Allgemeine Materialwissenschaft
Technische Fakultät, University of Kiel
Kaiserstasse 2, 24143 Kiel (Germany)

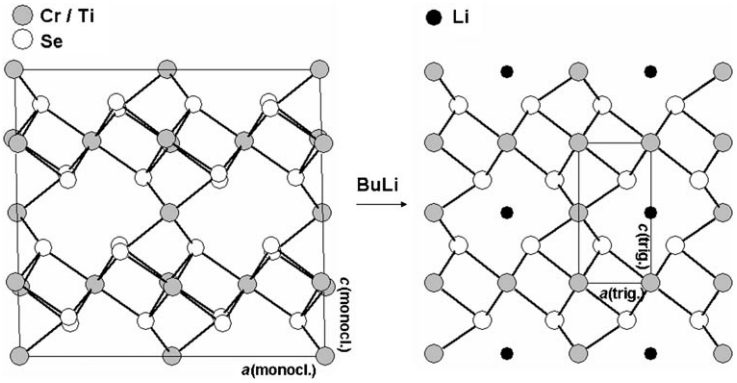

Figure 1. Crystal structures of monoclinic Cr_4TiSe_8 and trigonal $Li_xCr_4TiSe_8$. View along the *b* axis. The trigonal sub-cell $Li_xCrTi_{0.25}Se_2$ used for the Rietveld refinement is marked.

in the past.[1,11,12] Nevertheless, very little is known about intercalation mechanisms in more complex chalcogenide hosts that exhibit additional transition-metal atoms in the van der Waals gap as well as in a ternary transition-metal compound, such as the pseudo-layered Cr_4TiSe_8.

Phase transitions of the host structure upon intercalation have been observed in several layered chalcogenides. These are often attributed to electronic rather than to geometrical reasons.[13,14] They usually feature a transition to another polytype by sliding of the slabs or a change of the coordination geometry around the transition metal, and consequently of the crystal field and the d-band splitting. Migrations of transition-metal cations to new sites in the layers (e.g. Ni in Li_xNiPS_3[15]) or into the van der Waals gap have also been observed (e.g. Cu in Li_xCuFeS_2[16]). However, this is not the case in the monoclinic-to-trigonal phase transition of Cr_4TiSe_8. It is accompanied by a change of the transition metal coordination from a distorted to a regular MSe_6 (M = Cr, Ti) octahedron and consequently by an increase in symmetry. Hypothetical $Li_{0.75}CrTi_{0.25}Se_2$, with Li in all octahedral voids, would exhibit a NiAs-type structure.

In situ energy-dispersive X-ray diffraction (in situ EDXRD) was shown to be a powerful tool for the investigation of kinetics of chemical intercalation reactions, such as metallocene intercalation in TMDCs[7] or tetraalkylammonium and K^+ intercalation in layered $MnPS_3$.[8] However, to the best of our knowledge, no EDXRD study has been reported so far on Li intercalation with BuLi. The Cr_4TiSe_8/$Li_xCrTi_{0.25}Se_2$ system is very favourable for an EDXRD study because the phase transition gives rise to a clear structural change during the Li insertion that can easily be probed with X-ray diffraction, despite the low scattering power of Li.

The comprehensive understanding of Li intercalation reaction mechanisms in such complex host systems is not only a purely academic challenge but might also lead to improved knowledge and application of Li intercalation chemistry in the field of rechargeable batteries. Herein, we report results of in situ X-ray diffraction (in situ XRD) studies of the chemical and electrochemical intercalation, and we also present a possible reaction mechanism that is supported by results of X-ray absorption measurements.

Results

Chemical intercalation: The phase transition from monoclinic to trigonal symmetry can easily be characterised with X-ray diffraction (XRD) methods.[9] In the region of the XRD pattern of the monoclinic host at $\approx 32°\ 2\theta$ four intensive reflections are observed, three of which were resolved with the laboratory XRD facilities. In EDXRD experiments, these reflections are not resolved by the energy-dispersive detector so there is only one broad maximum. As lithiation proceeds, this maximum loses intensity and a new reflection appears at lower energy corresponding to the newly developing trigonal phase (Figure 2).

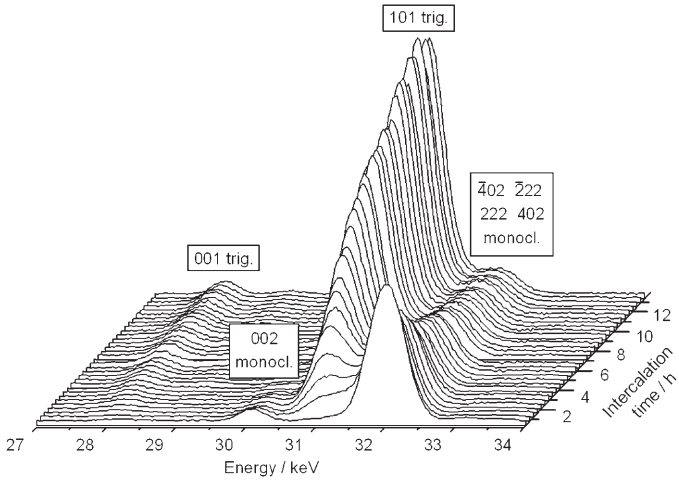

Figure 2. Three-dimensional view of the evolution of characteristic X-ray peaks during chemical Li intercalation of Cr_4TiSe_8 with BuLi at 60 °C used to monitor the phase transition. The reflection quartet of the monoclinic phase is not resolved by the energy-dispersive detector.

The intensities of these characteristic peaks were used for the kinetic evaluation of the chemical intercalation. The extent of the reaction, α, was determined from extrapolation of the intensity data to $t = \infty$. The α versus time curves are shown in Figure 3a for reaction temperatures of 20 °C (RT) and 60 °C. It can be seen that the phase transformation starts immediately at the beginning of the reaction and at 60 °C it is faster than at 20 °C. In both experiments, an "inactive fraction" of the genuine monoclinic material remains present, even after long reaction times. A phase mixture with roughly 20 % of the monoclinic phase was extrapolated for $t = \infty$. Note that, for the kinetic evaluation, the extent of reaction, α, was corrected for the inactive monoclinic fraction. The kinetic parameters were obtained by applying the Avrami–Erofëev equation in the form of a Sharp–Hancock plot[17] (Figure 3b) from the slopes and intercepts of the linear part of the curves. The results are summarised in

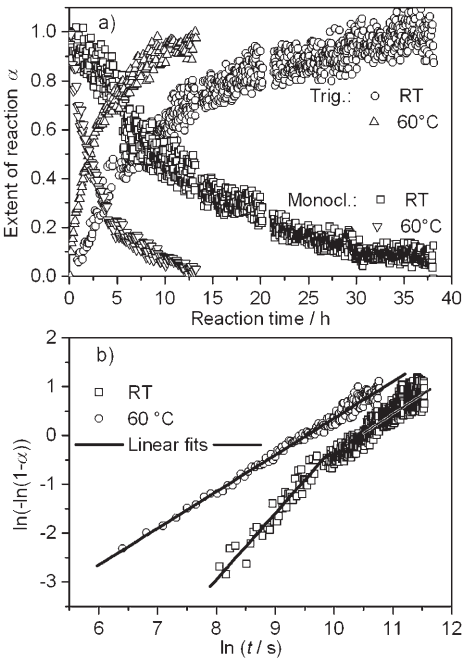

Figure 3. Intensity data of the monoclinic and trigonal phases for the chemical intercalation reactions at room temperature (RT) and 60 °C. a) Extent of reaction α versus time curve. b) Sharp–Hancock plot for kinetic evaluation. Missing data point (e.g. ≈21 h at RT) is caused by closed beam-shutters resulting from the injection process at the synchrotron facility.

Table 1. Kinetic parameters of the Li intercalation reaction of Cr_4TiSe_8 at room temperature (RT) and 60 °C obtained from the slopes and intercepts of the linear parts of the curves in the Sharp–Hancock plot (Figure 3b).

	α	m	k [s^{-1}]	$t_{0.5}$ [s^{-1}]
RT	0–0.45	1.35(7)	$3.6(6)\times10^{-5}$	≈30000
	0.6–1	0.79(3)	$2.7(3)\times10^{-5}$	
60 °C	0–1	0.75(1)	$6.8(2)\times10^{-5}$	≈8000

Table 1. A two-step mechanism was found for the reaction at 20 °C, which is seen in the Sharp–Hancock plot as two linear parts. The initial part of the reaction is of higher order and occurs faster. The half-life, $t_{0.5}$, is almost four times longer at room temperature than at 60 °C. Furthermore, only one mechanism seems to dominate for the whole reaction at 60 °C.

The evolution of the *d*-spacing and the full width at half maximum (FWHM) of the vanishing monoclinic quartet for the genuine phase and for the newly developing (101) reflection for the product phase is shown in Figure 4 for the experiment performed at 60 °C. The *d*-spacing for the reflections of the monoclinic phase increases in two linear steps during the reaction (Figure 4a). The shift is faster at the beginning and slows down after about 2 h ($\alpha\approx0.5$). Simultaneously, the profile width increases linearly over the whole reaction time (Figure 4b). The *d*-spacing of the (101) reflection of the trigonal material is enlarged by Li intercalation; however, this enlargement is saturated after approximately 4 h (Figure 4c), which is ≈6 h before the increase of intensity is saturated. The decrease of the FWHM (Figure 4d) also proceeds in a non-linear manner.

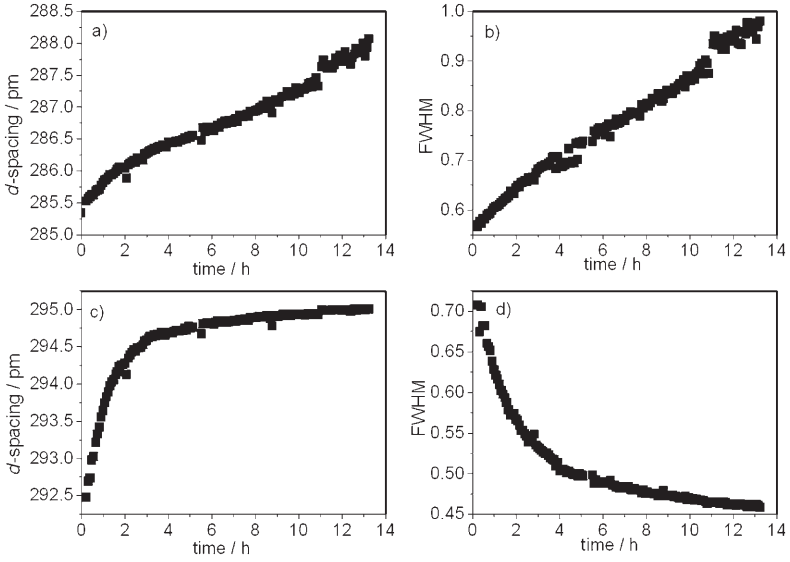

Figure 4. Evolution of the peak positions (a, c) and half-widths (b, d) of the (−402)/(−222)/(222)/(402) quartet of the monoclinic phase and the (101) reflection of the trigonal phase on the energy scale during the chemical intercalation with BuLi at 60 °C.

Electrochemical intercalation: In the electrochemical intercalation, the reaction can be monitored as a function of x in $Li_xCr_4TiSe_8$ because the degree of intercalation is directly related to the reaction time if a constant current is applied. According to Gibb's phase rule, the cell potential versus x curve should exhibit a constant voltage when two phases coexist in the intercalation electrode.[18] The cell potential was monitored in an overview measurement for $0<x<3$ (Figure 5). The open-circuit voltage of the cell was 2.3 V. The voltage drops at the early stages of the discharge process to reach a plateau of 1.5 V at approximately $x\approx0.1$. This voltage stays constant up to $x\approx0.7$ where a second drop is detected. For $x>0.9$, the cell potential is again constant at 0.8 V. To understand these features, the first part of the intercalation with the two voltage drops and the first plateau ($0<x<1.1$) were investigated with in situ XRD.

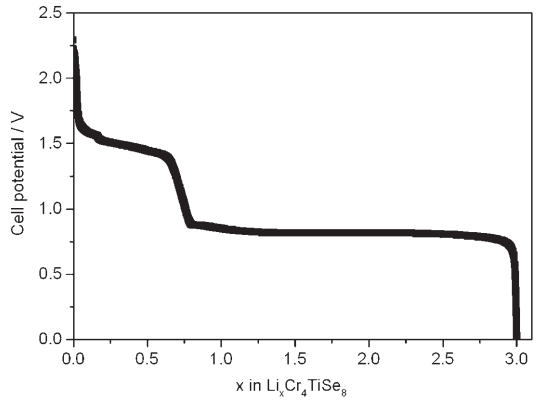

Figure 5. Cell potential of the electrochemical intercalation of Cr_4TiSe_8 versus Li content. Because there are inactive areas of the intercalation electrode, the end of the reaction is normalised to the theoretical final composition $Li_3Cr_4TiSe_8$.

The XRD data clearly show that two phases co-exist for $x>0.1$. The reflection intensities of the monoclinic phase $Li_xCr_4TiSe_8$ start to decrease linearly at $x>0.1$, whereas those of the trigonal phase $Li_xCrTi_{0.25}Se_2$ ($x = x'/4$) increase at this x value (Figure 6a). The monoclinic phase vanishes; however, an inactive fraction of $\approx 14\%$ is still present after the reaction, which was determined by Rietveld refinement of ex situ XRD data after intercalation with $x = 3.0$ (not shown). The unit-cell volumes and lattice parameters of the monoclinic and trigonal phases obtained from Rietveld refinement are shown in Figure 6b,c as a function of x.

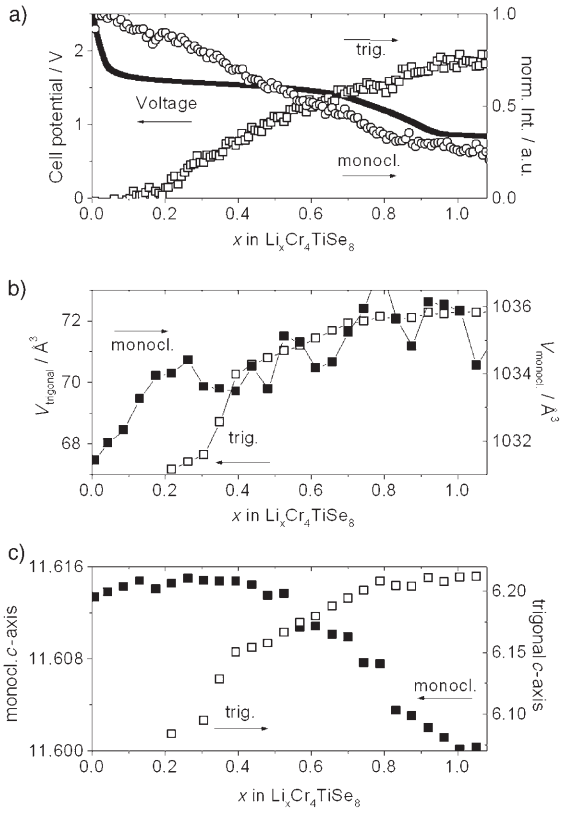

Figure 6. Electrochemical and XRD data for the first part of the intercalation reaction. Cell voltage and intensity data of the (002) and (001) reflections for the monoclinic and trigonal phase, respectively, versus composition (a); evolution of the unit cell volumes (b) and of the c axes (c) of the monoclinic and trigonal phases as obtained from Rietveld refinement. Lines are guides for the eyes.

X-ray absorption near-edge structure (XANES): X-ray absorption experiments at the Cr and Ti K-edges were performed on phase-pure trigonal samples $Li_xCrTi_{0.25}Se_2$ to determine variations of the valence of Cr and Ti as a function of x. The energy thresholds of the Ti and Cr K-edges are consistent with the valence state of the metals. XANES spectra of the host and the fully intercalated sample are shown in Figure 7a,b. Although the effect is weak, a clear trend can be seen in Figure 7c. The absorption-edge energies decrease with increasing Li content on account of a better screening of the core levels by a higher valence-electron density, which indicates a reduction of both metals. The Ti K-edge exhibits a shift for samples with $x< 0.84$ and remains approximately constant for $x>0.84$, whereas the K-edge of Cr is constant for small x and decreases significantly for $x>0.84$.

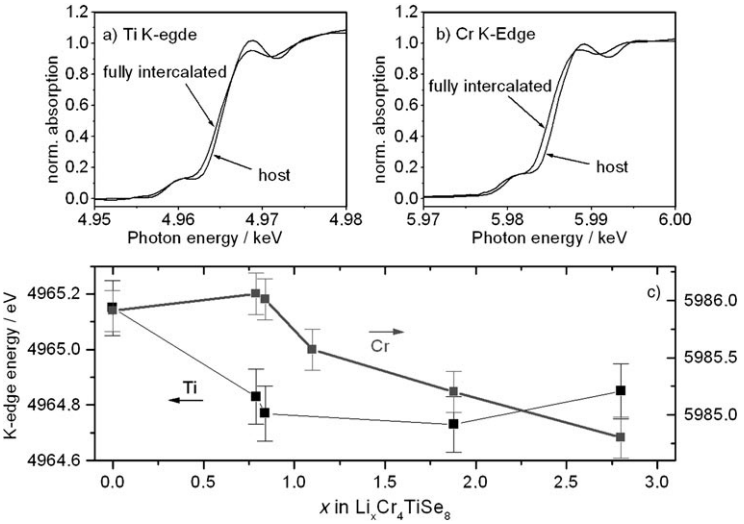

Figure 7. XANES spectra of the host and the fully intercalated material at the a) K-edge of Ti and b) K-edge of Cr. c) Absorption-edge energies for $Li_xCrTi_{0.25}Se_2$ samples as a function of x'.

Discussion

In a simplified description, the reaction mechanism of alkali-metal intercalation in layered hosts can be divided into several general steps: adsorption of the guest on the surface of the host, opening of the van der Waals gap, nucleation and growth of the intercalated phase and finally diffusion of the guest into the bulk of the host.[5,7,19] The kinetics of the reaction are then determined by the rate-limiting step

of the intercalation reaction. It is also obvious from the complex nature of the intercalation reaction that the evaluation of the experimental data cannot yield an unambiguous interpretation of the kinetic data obtained by fitting the data with Avrami-type expressions or by the use of the Sharp–Hancock approach.

The kinetics of the chemical intercalation reaction of Cr_4TiSe_8 in BuLi at room temperature obeys a two-step mechanism. In the first stage ($\alpha \approx 0.45$), the reaction exponent (m) is 1.35(7), which may suggest phase-boundary control (kinetic models R2; R3, $m_{theo} = 1.10$; 1.06). However, as mentioned above, intercalation is complex and the validity of the kinetic models is related to several strict conditions, that is, it is assumed that the particles are uniformly shaped and have the same size.[20] These conditions are seldom fulfilled in real reaction systems and thus an agreement between experimental and theoretical parameters cannot always be achieved. If phase-boundary control is assumed, the rate of Li intercalation in Cr_4TiSe_8 is governed by the movement of the monoclinic/trigonal phase boundary in the first half of the reaction. Thus, the structural rearrangement of the host matrix is the rate-limiting step. For $\alpha > 0.6$, the value for m of 0.79(3) differs from values reported from theoretical models. However, the decrease of m might be interpreted as a change of the rate-limiting step towards diffusion control (kinetic models D1–D4, $m_{theo} =$ 0.53–0.60). Hence, it is likely that the diffusion of Li into the bulk of the host becomes rate-limiting in the later stages of the reaction. The phase transition is most probably driven electronically,[9] and the transfer of electrons is a prerequisite for the rearrangement of the host structure. The transfer of electrons and consequently the movement of the phase boundary must be associated with the diffusion of charge-compensating Li^+ ions. As the reaction proceeds, diffusion of Li^+ into the bulk is the "bottleneck" of the reaction and the structural rearrangement is only of secondary importance.

A change of the parameter m towards lower values was also found by EDXRD for the intercalation of cobaltocene in layered SnS_2 and $SnSe_2$.[7] The authors proposed a model that assumes a much faster 2D diffusion of cobaltocene inside the van der Waals gaps compared to the formation of new nucleation sites at the edges of the crystals, that is, the distinct layers are filled instantaneously. In this case, the process which is determined by applying the Avrami–Erofféev equation is not a 2D diffusion but rather a 1D diffusion of filled layers parallel to the stacking axis. Furthermore, intercalation in a distinct layer is assumed to favour intercalation into the neighbouring layer. A simulation on the basis of this model, which accounts for the varying probabilities of imaginary blocks in the host crystal to be intercalated, successfully reproduced the kinetic results.[7] For the present compound, two-step kinetics is also observed, but for a very different intercalation system in terms of the guest species and the 3D host matrix.

For the reaction at 60 °C, no two-step behaviour occurred and the value for m of 0.75(1), which is close to that in the second part of the room temperature reaction, indicates isokinetic behaviour. Obviously, the increase in the reaction temperature by 40 °C seems to favour short-range atomic shifts in the host lattice, which are associated with the structural rearrangement for the long-range solid-state diffusion of Li. This is consistent with the observation that although fully intercalated, phase-pure trigonal samples are not accessible at room temperature, they can be prepared at temperatures close to 60 °C.[9]

The half-life of the reactions indicates that Li intercalation is relatively slow in Cr_4TiSe_8 compared to other transition-metal chalcogenide systems. One explanation for this is that in the present host, intercalation is hampered by Cr atoms residing in the van der Waals gaps. The slabs are pinned together by Cr–Se interactions of these atoms and also by weak inter-layer Cr–M (M = Cr, Ti) bonding. This effect of additional metal atoms in the van der Waals gaps was also observed for electrochemical[21] and chemical[22] intercalation of Li into metal-rich $Ti_{1+y}S_2$, which is less straightforward than for the stoichiometric host.

The profile width of the Bragg reflections is related to strain and to crystallite size effects. Both effects play a role in this reaction system. The average monoclinic and trigonal domain size varies during the reaction, and the strain was found to accompany Li intercalation,[9] as can be expected for a structural rearrangement at low temperatures. Directly after nucleation, the lithiated domains are very small and grow fast. This explains the sharp decrease of the FWHM for the trigonal domains at the beginning of the reaction (Figure 4d). The increase in the FWHM of the monoclinic reflections is related to the strain that arises when Li insertion destabilises the monoclinic structure (Figure 4b).

The phase transition was not complete for all reactions performed, and a significant inactive fraction of the host material could be identified at the end. This might be attributable to defects in the structure of the host. Shear defects may give rise to incomplete intercalation in three-dimensional hosts because they may block the void tunnels and consequently some parts of the host would remain inaccessible for intercalation.[23] The electrode material was sintered for several days and can be assumed to exhibit fewer defects. Hence, the inactive fraction is smaller for electrochemical intercalation. Phase-pure trigonal samples can be prepared in BuLi at 60 °C in 3 days.[9]

The electrochemical data show that, in the early stages of the intercalation, the monoclinic host is intercalated without a phase transition. The cell voltage drops for $0 < x < 0.1$ from 2.3 to 1.5 V, indicating a single-phase region in monoclinic $Li_{x<0.1}Cr_4TiSe_8$. The first voltage plateau at 1.5 V ($0.1 < x < 0.7$) is clearly attributable to the two-phase region. The composition $Li_{0.1}Cr_4TiSe_8$ seems to be critical for the phase transition. For $x > 0.1$, every new intercalated Li^+/electron forces the phase transition. According to the results of the Rietveld refinement, an increase of the monoclinic unit cell volume of 0.25% occurs for the initial part of the intercalation and a further increase of only 0.13% is found for the rest of the reaction ($0.1 < x < 3.0$), indicating a dra-

matic deceleration in the rate of expansion in the two-phase region (Figure 6b). These results suggest that the degree of intercalation of the monoclinic phase does not significantly exceed $x = 0.1$, and all monoclinic material remains near the critical composition $Li_{0.1}Cr_4TiSe_8$ for the rest of the reaction. The same effect might be responsible for slowing down the shift of the monoclinic reflection quartet found in the chemical intercalation reaction at $\alpha \approx 0.5$ (Figure 4a). Interestingly, despite the small changes of the cell volume of the monoclinic material for $x > 0.1$, larger changes of the lattice parameters can still be observed. A decrease in the monoclinic c axis commences with the phase transition (Figure 6c); however, shrinking is outbalanced by the increase of the a and b axes, resulting in an almost constant unit-cell volume. In contrast to the c axis, the a and b axes and the monoclinic angle do not show any discontinuous behaviour near the critical composition $x = 0.1$ (not shown). The length of the c axis becomes even smaller than the initial value in the host material. This might be attributed to the partial formation of Ti^{III} centres by the reduction caused by electron transfer from Li to the host. The d^1 centres of Ti^{III} are able to form bonds with Cr^{III} in the van der Waals gap across the MSe_6 octahedra sharing common faces. These short inter-layer M–M contacts are orientated parallel to the c axis, which explains the shrinkage of this axis. However, with respect to the time-dependence of this phenomenon, other electronic contributions as well as structural relaxation and non-equilibrium effects may also play a role. For instance, one can imagine that Li^+ ions first reside not on the octahedral sites and during relaxation they move from this site reaching finally the equilibrium position. Such a structural effect would explain the fact that the c axis remains nearly constant during the early stages of intercalation, despite electron uptake by the host material.

The increase of the unit-cell volume of the newly developing trigonal phase for $x > 0.1$ (Figure 6b) is a typical feature of intercalation reactions. The enlargement is fast at the beginning and is already complete at $x = 0.8$, which is in the regime of the second voltage drop. Such saturation is often observed in TMDC/Li intercalation systems (e.g. Li_xTiS_2[24,25]). In $Li_xCrTi_{0.25}Se_2$, the increase of a and c is about 2.5% for both axes. Usually, the expansion of the c axis is much greater than that of the a parameter for layered hosts. However, $Li_xCrTi_{0.25}Se_2$ is only a pseudo-two-dimensional material and, therefore, the lattice expansion proceeds in a 3D fashion.

From the XRD data, a second single-phase region can clearly be ruled out for the compositional range $0.7 < x < 0.9$, where the step of the cell potential is found. Drops in the electrochemical cell potential that are not attributable to a single-phase region have previously been reported, for example, for the Chevrel intercalation compounds $Li_xRu_zMo_{6-z}Se_8$ and the corresponding Li content x was also shown to depend on the ratio of the transition metals.[26] In these systems, they were attributed to the passage of the Fermi energy through a band gap. Conductivity measurements are underway to check whether this might also play a role in the $Li_xCr_4TiSe_8$ system. Another possible reason for an abrupt voltage drop is that a particular site in the host has been completely filled and another site with higher lattice-site energy is now being filled.[12]

In an analogous electrochemical experiment[27] with the host material $Cr_3Ti_2Se_8$, which exhibits a very similar structure and the same phase transition during Li intercalation,[28] the cell voltage was found to drop at a composition close to $Li_2Cr_3Ti_2Se_8$. From this result, it is tempting to relate the voltage step directly to y in $Cr_{5-y}Ti_ySe_8$, that is, to the Ti content of the host material. The second voltage drop can then be assumed to be caused by the complete reduction of Ti, which would be the first redox chemical step in the intercalation reaction. This is consistent with the results of the XANES measurements, in which the reduction of Ti is found to occur prior to the reduction of Cr upon Li intercalation (Figure 7c). In an ionic picture, the host compound can be written as $(Cr^{+III})_4(Ti^{+IV})(Se^{-II})_8$.[10] Assuming a formula of $(Li^{+I})(Cr^{+III})_4(Ti^{+III})(Se^{-II})_8$ after the intercalation of one Li, the XANES results suggest $(Li^{+I})_x(Cr^{+III})_{5-x}$-$(Cr^{+II})_{x-1}(Ti^{+III})(Se^{-II})_8$ for $1 \le x \le 3$.

The question still arises as to whether an ionic picture is appropriate to account for the electronic situation. Unfortunately, calculation of the electronic band structure of Cr_4TiSe_8 is not straightforward owing to its open nature and the large number of atoms in the unit cell. Localised d-electron states on Cr were observed in K_xCrSe_2[29] and $Na_{x>0.6}CrSe_2$,[30] whereas non-intercalated $CrSe_2$ exhibits delocalised d states.[30] Delocalisation or partial delocalisation is discussed for Cr_5Se_8[31] (V_5S_8 structure type) and $Li_xTi_{1-y}Cr_yS_2$.[32] Deintercalated $TlCr_5Se_8$[33] (TlV_5S_8 structure-type) as well as our host compound exhibit localised magnetic moments. It was shown for Li intercalation in $ZrSe_2$ that the lattice parameters hardly change as the intercalated electrons fill localised levels whereas they expand significantly when delocalised bands are filled.[12,34,35] Because the lattice expansion is saturated at $x \approx 1$ ($x \approx 2$ for $Cr_3Ti_2Se_8$[27]), we believe that for $0 < x < 1$ the delocalised d band of Ti is filled whereas for $1 < x < 3$ localised Cr levels are occupied. This effect might also give rise to the early saturation of the d-spacing shift during the intercalation with BuLi (Figure 4c).

Conclusion

On the basis of our results, we propose the following reaction mechanism for the intercalation of Li into Cr_4TiSe_8: in the first step, Cr_4TiSe_8 is intercalated with approximately 0.1 Li to form monoclinic $Li_{0.1}Cr_4TiSe_8$. Above this critical Li content, a phase transition sets in and domains of trigonal $Li_{x'>0.025}CrTi_{0.25}Se_2$ ($x' = x/4$) nucleate and grow. The two phases co-exist during the whole reaction ($0.1 < x < 3.0$). The first redox centre that accepts electrons during the intercalation process is Ti^{IV}, which is completely reduced to Ti^{III} at $x = 1$. Further intercalation leads to the formation of Cr^{II}. At the end of the reaction, all the monoclinic material should

be transformed into the trigonal phase and all void octahedral sites in the host structure should be filled at $x = 3.0$. However, the experimental results demonstrate that the final composition could not be reached owing to inactive fractions of the host material.

In situ EDXRD was used for the kinetic evaluation of the chemical intercalation with BuLi. A two-step mechanism was found for the reaction at room temperature. The decrease of the reaction exponent m was attributed to the change from phase-boundary control to diffusion control for a reacted fraction of $\alpha \approx 0.5$. A single-step diffusion-controlled mechanism was found for the intercalation at 60 °C.

Experimental Section

Synthesis of the host compound: Cr_4TiSe_8 was prepared from the elements in evacuated quartz ampoules at 950 °C. It was obtained as a grey powder of plate-like crystallites. Phase pureness was checked with powder X-ray diffractometry on a STOE Stadi-P diffractometer ($Cu_{K\alpha}$ radiation) equipped with a Ge monochromator and a position-sensitive detector (PSD) in a transmission geometry. Rietveld refinement of the single-crystal data[10] as a structural model resulted in R factors better than 8% for all samples. The synthesis, as well as the structural and magnetic properties of the host compound are described in detail elsewhere.[10]

Chemical intercalation: The host compound was sieved prior to intercalation to guarantee a uniform distribution of the grain size between 73 and 100 μm. These grains are agglomerates of crystallites with sizes ranging from 5 to 20 μm. 50 mg portions of Cr_4TiSe_8 were then weighed into test tubes that were then sealed with screw caps. The tubes were filled with an inert atmosphere in an Ar glove-box and closed with a plug. EDXRD experiments were performed with the F3 beamline of HASYLAB at DESY, Hamburg (Germany). This beamline is equipped with an energy-dispersive detector that allows fast recording of the diffraction patterns. The intensity of the incoming "white" synchrotron beam was sufficient to penetrate the tube walls. The experimental set-up, its applicability for in situ EDXRD measurements and the procedures of data treatment were described in detail elsewhere.[36,37] Butyllithium (BuLi) in hexane (2 mL, 1.6 M in hexane) was injected into the tubes through the plug directly before the experiment was carried out. After removal of the cannula, the screw cap was placed on the tube to prevent the plug from being pushed upwards in case of an autogenous pressure in the tube. The tubes were placed in a combined heating and magnetic stirring device described elsewhere.[36] Diffraction patterns of the reaction mixture were recorded every 3 min. The diffracted intensities of the starting material and product phases were evaluated as a function of the reaction time. The intensity of the Se Kβ fluorescence peak was used for normalisation to account for variations in the amount of sample in the beam and for the intensity of the incoming synchrotron beam.

Electrochemical intercalation: Cr_4TiSe_8 powder (≈100 mg portions) was compacted to pellets with a diameter of 8 mm. No additives were used to improve adhesion or conductivity. The pellets were sintered for 3 days at 540 °C in a reduced Ar atmosphere. The pellets were used as insertion electrodes in a custom-built electrochemical in situ cell made of Teflon (Figure 8). In this cell, the host pellet is located on a height-adjustable Mo stage (5 mm in diameter) so that it is in contact with the electrolyte ($LiClO_4$ in ethylene carbonate and 1,2-dimetoxyethane, 1:1) from underneath and from the sides. Two pieces of Li act as counter-electrode and a reference electrode. The cell was prepared in an Ar glove-box and sealed with PE foil that was tautened and fixed with an O ring. The cell was mounted on a Bruker D8-Advance θ–θ diffractometer equipped with a Göbel mirror ($Cu_{K\alpha}$ radiation), a scintillation counter and a height-adjustable sample stage. The electrodes were connected to the current source (Keithley 2400 SourceMeter) and the measurement unit (Keithley 2000 Multimeter). XRD patterns of the host electrode were recorded with this set-up every 20 min during the electrochemical intercalation process. The current was held constant at 100 μA and the cell voltage was measured every 30 s and recorded with the custom-made software KEI V8.0.[38] Only the initial part of the electrochemical intercalation was performed in the in situ cell. An overview measurement of the complete reaction was carried out in the Ar glove-box.

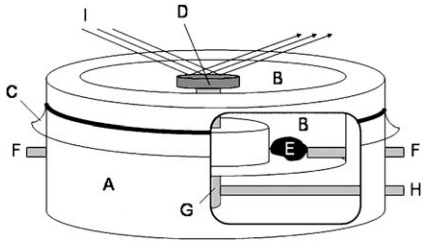

Figure 8. The custom-built electrochemical cell for in situ XRD consists of a Teflon body (A) and the electrolyte room (B), which is sealed by X-ray transparent PE foil (C) after preparation. The host pellet (D) is located in the electrolyte directly below the foil. Pieces of Li (E) act as a counter-electrode and a reference electrode. Mo screws (drawn in light grey) are used to fix and connect the Li electrodes (F). The central screw (G) allows the height adjustment of the pellet, which is connected via another screw from the side (H). The cell was mounted on a θ–θ diffractometer and XRD patterns (I) were recorded in situ during electrochemical intercalation.

Rietveld refinement: Powder patterns of the electrochemically intercalated electrode material were recorded ex situ after intercalation with the STOE Stadi-P in a transmission geometry. The samples were protected from the atmosphere by sealing the sample holder with X-ray transparent foil. The 2θ range was 10–90° 2θ with a step width of 0.01° 2θ. The counting time per step was typically ≈1 h. Rietveld refinements of the patterns were carried out with the program package FULLPROF.[39] The background was treated by linear extrapolation between manually selected points. The reflection profiles were modelled with Thompson–Cox–Hastings pseudo-Voigt functions with three parameters. Preferred orientation was included by means of the March–Dollase function. The zero point was refined as a global parameter.

For the in situ data recorded on the Bruker D8-Advance, the 2θ range was 10–70° 2θ and the step width 0.05° 2θ. The quality of the patterns suffered from short counting times of 1 s per step that were applied to guarantee a sufficient resolution on the time-scale. Severe (001) texture owing to the preferred orientation of the grains was present in the in situ XRD patterns. Consequently, the Rietveld refinement yielded R factors of ≈15% for the single patterns. Although the absolute structural data might thus be imprecise, the variation of the lattice parameters during intercalation is clearly probed by the Rietveld results. The data was shifted to a reliable absolute scale by normalising the lattice parameters of the monoclinic phase obtained from the first in situ pattern to the ex situ results of the pure host compound.

X-ray absorption near-edge structure (XANES): XANES measurements were performed at the beamline E4 of HASYLAB, Hamburg (Germany). The samples were thoroughly ground and pressed into pellets with cellulose. Spectra of the K-edges of Ti and Cr were recorded with a transmission geometry in ionisation chambers. Reference spectra of elemental Ti and Cr foil, respectively, were recorded simultaneously and used for energy calibration. For this purpose, a sharp feature slightly above the threshold energy was used for a reliable and comparable calibration among the samples, but it lead to a small shift of the absolute energy scale. The edge positions were determined by the root of the second derivative of the XANES spectra. WinXAS[40] software was used for evaluation. Phase-pure trigonal samples of $Li_xCrTi_{0.25}Se_2$ for XANES experiments were obtained by full intercalation at elevated temperatures and subsequent Li removal in water[9] The fully intercalated sample was shown to have a Li content of $x = 2.79$ by atomic absorption spectrosco-

py (AAS, Perkin Elmer AAnalyst 300). After water treatment for 0.5, 24 and 96 h, samples with intermediate Li contents of $x = 1.10$, 0.84 and 0.79, respectively, were obtained. Immediate filtration (less than 1 min of water treatment) yielded a sample with $x = 1.88$. The noise on the Ti XANES of the $Li_{0.28}CrTi_{0.25}Se_2$ sample was too strong to determine a reliable edge position.

Acknowledgements

Helpful discussions with C. Knittlmayer of Prof. W. Weppner's group are greatly acknowledged. We thank Dr. K. Klemtentiev of HASYLAB for his support and also DESY for allocation of beam time. R. Sievertsen, M. Wegner, S. Keipert, and M. Rolff have contributed in their research project for diploma students at the University of Kiel. We acknowledge financial support by the State of Schleswig-Holstein, and the Deutsche Forschungsgemeinschaft (DFG).

[1] R. Schöllhorn, *Angew. Chem.* **1980**, *92*, 1015–1035; *Angew. Chem. Int. Ed. Engl.* **1980**, *19*, 983.
[2] A. J. Jacobsen in *Solid State Chemistry: Compounds* (Ed.: A. K. Cheetham, P. Day), Oxford University Press, Oxford (UK), **1992**, pp. 182–233.
[3] J. V. Acrivos in *Intercalated Layered Materials* (Ed.: F. A. Lévy), D. Reidel Publishing Company, Dordrecht (NL), **1979**, pp. 33–98.
[4] R. Schöllhorn, *Comments Inorg. Chem.* **1983**, *2*, 271–292.
[5] R. R. Chianelli, J. C. Scanlon, B. M. L. Rao, *J. Solid State Chem.* **1979**, *29*, 323–337.
[6] F. Ronci, P. Reale, B. Scrosati, S. Panero, V. Rossi Albertini, P. Perfetti, M. di Michiel, J. M. Merino, *J. Phys. Chem. B* **2002**, *106*, 3082–3086.
[7] J. S. O. Evans, S. J. Price, H.-V. Wong, D. O'Hare, *J. Am. Chem. Soc.* **1998**, *120*, 10837–10846.
[8] D. O'Hare, J. S. O. Evans, R. Francis, S. Price, S. O'Brien, *Mater. Sci. Forum* **1998**, *278–281*, 367–378.
[9] M. Behrens, O. Riemenschneider, W. Bensch, S. Indris, M. Wilkening, P. Heitjans *Chem. Mater.* **2006**, *18*, 1569–1575.
[10] W. Bensch, B. Sander, C. Näther, R. K. Kremer, C. Ritter, *Solid State Sci.* **2001**, *3*, 559.
[11] M. S. Whittingham, *Prog. Solid State Chem.* **1978**, *12*, 41–99.
[12] J. Rouxel, *J. Chim. Pys.* **1986**, *83*, 841–850.
[13] E. Sandré, R. Brec, J. Rouxel, *J. Solid State Chem.* **1990**, *88*, 269–277.
[14] R. Brec, E. Prouzet, G. Ouvrard, *J. Power Sources* **1993**, *43*, 277.
[15] R. Brec, *Solid State Ionics* **1986**, *22*, 3.
[16] R. Fong, J. R. Dahn, *Phys. Rev. B* **1989**, *39*, 4424.
[17] J. D. Hancock, J. H. Sharp, *J. Am. Ceram. Soc.* **1972**, *55*, 74–76.
[18] W. R. McKinnon in *Solid State Electrochemistry* (Ed.: P. G. Bruce), Cambridge University Press, Cambridge (UK) **1995**, pp. 163–198.
[19] R. Schöllhorn, *Pure Appl. Chem.* **1984**, *56*, 1739–1752.
[20] a) M. Avrami, *J. Chem. Phys.* **1939**, *7*, 1103–1112; b) M. Avrami, *J. Chem. Phys.* **1940**, *8*, 212–224; c) M. Avrami, *J. Chem. Phys.* **1941**, *9*, 177–184.
[21] A. H. Thompson in *Fast Ion Transport in Solids* (Eds.: P. Vashishta, J. N. Mundy, G. K. Shenoy), Elsevier North Holland Inc., Amsterdam (NL) **1979**, pp. 47–51.
[22] M. B. Dines, *Mater. Res. Bull.* **1975**, *10*, 287–291.
[23] R. Schöllhorn, W. Schramm, *Z. Naturforsch. B* **1979**, *34*, 697.
[24] M. S. Whittingham, F. R. Gamble, *Mater. Res. Bull.* **1975**, *10*, 363–371.
[25] J. R. Dahn, D. C. Dahn, R. R. Hearing, *Solid State Commun.* **1982**, *42*, 179–183.
[26] W. R. McKinnon, L. S. Selwyn, *Phys. Rev. B* **1987**, *35*, 7275–7278.
[27] J. Wontheu, M. Behrens, W. Bensch, S. Indris, M. Wilkening, P. Heitjans, unpublished results.
[28] J. Wontcheu, W. Bensch, *Z. Kristallogr*. **2005**, *185*, *Suppl. 22*, (Abstract, Conference Contribution to the 13. Jahrestagung der Deutschen Gesellschaft für Kristallographie (DGK), Köln (Germany), **2005**).
[29] G. A. Wiegers, *Physica B* **1980**, *99*, 151–165.
[30] C. F. van Bruggen, R. J. Haange, G. A. Wiegers, D. K. G. de Boer, *Physica B* **1980**, *99*, 166–172.
[31] A. W. Bither, W. Sleight, T. A. Bither, *Inorg. Chem.* **1969**, *8*, 566–569.
[32] J. M. Tarascon, F. J. DiSalvo, M. Eibschutz, D. W. Murphy, J. V. Waszczak, *Phys. Rev. B* **1983**, *28*, 6397–6406.
[33] W. Bensch, B. Sander, O. Helmer, C. Näther, F. Tuczek, A. Panich, A. Shames, *J. Solid State Chem.* **1999**, *145*, 235–246.
[34] Y. Onuki, T. Hirai, K. Shibutami, T. Komatsubara, *J. Inclusion Phenom.* **1984**, *2*, 279.
[35] C. Berthier, Y. Chabre, P. Segransan, P. Chevalier, L. Trichet, A. Lé Méhauté, *Solid State Ionics* **1981**, *5*, 379.
[36] L. Engelke, M. Schaefer, M. Schur, W. Bensch, *Chem. Mater.* **2001**, *13*, 1383–1390.
[37] L. Engelke, M. Schaefer, F. Prosch, W. Bensch, *Eur. J. Inorg. Chem.* **2003**, 506–513.
[38] O. Riemenschneider, PhD Thesis, University of Kiel (Germany), **2004**.
[39] J. Rodriguez-Carvajal, FULLPROF, Lab. Leon Brillouin, Gif-sur-Yvette Cedex (France), **2005**.
[40] T. Ressler, WinXAS 3.1, **2004**.

Received: November 25, 2005
Revised: February 17, 2006
Published online: May 24, 2006

